

RESEARCH

Open Access



An electrochemical biosensor for the detection of microRNA-31 as a potential oral cancer biomarker

Sanket Naresh Nagdeve¹, Bavithira Suganthan¹ and Ramaraja P. Ramasamy^{1*}

Abstract

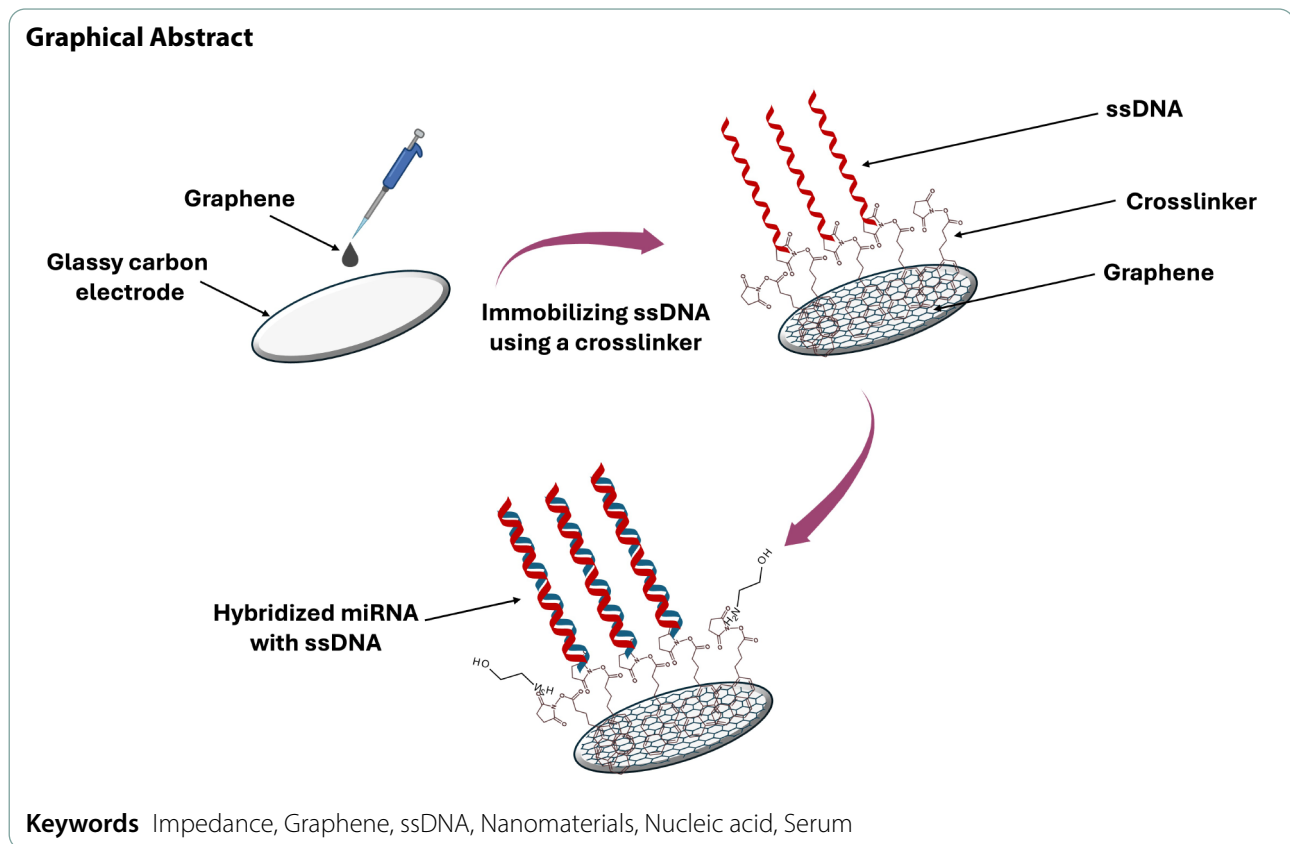
Oral cancer presents substantial challenges to global health due to its elevated mortality rates. Approximately 90% of these malignancies are oral squamous cell carcinoma (OSCC). A significant contributor to the prevalence of oral cancer is the difficulty in detecting cancerous biomarkers, further exacerbated by socioeconomic disadvantages and late-stage diagnoses. Given the critical nature of oral cancer, the early detection of biomarkers is essential for reducing mortality rates. This study investigates the application of microRNA-31 (miRNA-31) as a biomarker for the electrochemical detection of oral cancer, recognizing the considerable potential that microRNAs have demonstrated in cancer screening and diagnosis. The methodology employed includes the use of a glassy carbon electrode modified with graphene and a molecular tethering agent designed to enhance sensitivity and specificity. The biosensor exhibited a limit of detection of 10^{-11} M (70 pg/mL or 6.022×10^6 copies/ μ L) in buffer and 10^{-10} M (700 pg/mL or 6.022×10^7 copies/ μ L) in diluted serum for the complementary target miRNA-31 using the Six Sigma method. The efficacy of this biosensor was further validated through specificity studies utilizing a non-complementary miRNA in both buffer and human serum samples. The electrochemical biosensor displayed exceptional performance and high sensitivity in detecting miRNA-31, confirming its role as an innovative sensor for the non-invasive diagnosis of oral cancer. Furthermore, the proposed biosensor demonstrates several advantages over current methodologies, including reduced detection time, and cost-effective reagents.

*Correspondence:
Ramaraja P. Ramasamy
rama@uga.edu

Full list of author information is available at the end of the article



© The Author(s) 2025. **Open Access** This article is licensed under a Creative Commons Attribution-NonCommercial-NoDerivatives 4.0 International License, which permits any non-commercial use, sharing, distribution and reproduction in any medium or format, as long as you give appropriate credit to the original author(s) and the source, provide a link to the Creative Commons licence, and indicate if you modified the licensed material. You do not have permission under this licence to share adapted material derived from this article or parts of it. The images or other third party material in this article are included in the article's Creative Commons licence, unless indicated otherwise in a credit line to the material. If material is not included in the article's Creative Commons licence and your intended use is not permitted by statutory regulation or exceeds the permitted use, you will need to obtain permission directly from the copyright holder. To view a copy of this licence, visit <http://creativecommons.org/licenses/by-nc-nd/4.0/>.



Introduction

Oral cancer represents approximately 3% of all cancer diagnoses in the United States and remains one of the most prevalent cancers globally [1]. According to the 2023 Global Cancer Observatory, lip and oral cancers account for 4,000 new cases and 100,000 deaths worldwide [2]. Oral squamous cell carcinoma (OSCC), constituting nearly 90% of oral cancers, is particularly aggressive and prone to metastasis, making early detection crucial. OSCC accounts for 40% of head and neck cancers and commonly affects the tongue, lips, floor of the mouth, buccal mucosa, and gums [3, 4]. Key risk factors for OSCC include tobacco use, alcohol consumption, betel quid chewing, and human papillomavirus (HPV) [5–7]. The delayed diagnosis of OSCC often results in poor outcomes, with many cases identified at advanced stages, leading to reduced treatment options and survival rates. Early detection has been shown to significantly reduce mortality in high-risk individuals, such as tobacco and alcohol users [8]. Recognizing symptoms such as erythematous or leukoplakic patches, ulcers, atypical hemorrhaging, or neoplasms within the oral cavity is essential for a prompt diagnosis. Timely intervention can elevate the survival rate to over 80%, thus ensuring an enhanced quality of life for patients.

Biomarkers are specific molecules that indicate the presence or progression of cancer. A variety of

biomarkers, including microRNAs (miRNAs), cytokines, and proteins, have demonstrated substantial potential in improving the early diagnosis and monitoring of disease progression in oral cancer [6, 8]. These biomarkers hold immense potential for advancing patient outcomes and facilitating personalized medical care. Among them, miRNAs have emerged as promising candidates for cancer screening and clinical diagnostics. Recent studies have identified the presence of miRNAs in various bodily fluids, thereby establishing their significance as valuable diagnostic and prognostic indicators [9]. These small molecules serve as non-invasive markers for the screening and early detection of oral cancer and pre-malignant conditions, where the dysregulation of miRNAs is closely linked to the development of malignancy.

Specifically, certain miRNAs have proven instrumental in identifying and monitoring OSCC progression [10]. Osan et al. discussed the potential of miRNAs as biomarkers for early detection, development and therapeutic targets in oral cancer and reported several key miRNAs including miRNA-21, miRNA-24, miRNA-31, miRNA-145, miRNA-196b, etc [11]. Yu et al. highlighted the critical role of miRNA-21 in promoting perineural invasion associated with poor survival rate in oral cancer patients [12]. He et al. also reported that the salivary exosomal biomarker miRNA-24 promoted the proliferation of

OSCC cells [13]. Similarly, miRNA-31 is upregulated in oral leukoplakia and OSCC, emphasizing its significance in these pathological conditions. Lu et al. identified circulating miRNA-31-5p as a potential biomarker and therapeutic target for oral cancer [14]. miRNA-31 functions as an oncogenic factor in the progression of OSCC and is significantly upregulated in the saliva, serum, and tumor tissue of OSCC patients. An increase in this biomarker has been reported in both saliva [15, 16] and serum samples when examined in the head and neck areas [17–19]. Serum presents elevated concentrations of cancer biomarkers as it captures systemic biomarkers that reflect physiological changes throughout the body, particularly at low levels [19]. Towle et al. reported the expression of miRNAs in the serum samples of patients to identify high-risk oral lesions prior to their clinical manifestation [20]. This makes serum an invaluable medium for the early diagnosis and monitoring conditions that may not be localized to a specific site. The consistent upregulation of miRNA-31 across various biological samples, especially serum, underscores its potential as a reliable biomarker for non-invasive diagnostics in oral cancer [21]. Therefore, an early screening test for miRNA-31 could serve as a preliminary indicator of oral cancer and assist in determining the necessity for further validation through established diagnostic methods.

The existing methodologies employed for detecting miRNAs as biomarkers for cancer include reverse transcriptase quantitative polymerase chain reaction (RT-qPCR), droplet digital PCR (ddPCR), and next-generation sequencing [14, 22]. However, these techniques require considerable labor, time, and expensive instruments [22–25]. In recent years, isothermal nucleic acid amplification techniques (NAATs) have emerged as alternatives, allowing for rapid detection without thermal cycling. However, they often require complex primer design, and expensive reagents. Moreover, improper primer design can lead to non-specific binding, resulting in unintended amplification and reduced assay specificity [26–29]. In contrast, biosensors offer a more advantageous alternative, providing reduced costs, enhanced sensitivity, and expedited results. These biosensors facilitate the detection of miRNAs with greater precision and swiftness, aligning with the demand for more efficient and timely cancer diagnostics [30, 31].

Biosensors have emerged as crucial instruments in the detection of miRNAs, which serve as significant biomarkers for various types of cancer, including oral cancer, particularly at low concentrations that are vital for early diagnosis [32–34]. Electrochemical biosensors offer a rapid, sensitive, and cost-effective method for the identification of miRNAs in biological fluids such as serum, thereby facilitating non-invasive cancer screening. This approach holds the potential to substantially reduce

mortality rates associated with oral cancer by enabling prompt diagnosis and intervention, thus rendering it exceptionally valuable in the realm of early clinical diagnostics [35].

Electrochemical Impedance Spectroscopy (EIS) is a highly sensitive technique for analyzing interfacial responses on electrode surfaces. It measures changes in electrochemical responses and provides information such as ohmic resistance of the electrolyte (R_s); the charge transfer resistance (R_{CT}), inversely related to the efficiency of electron transfer at the interface; a double-layer capacitance (C_{DL}) for surface properties of the electrode, such as the formation of an electrical double layer and Warburg impedance (Z_W) for ions diffusing from the bulk solution to the surface of the electrode in a Nyquist plot. EIS can detect miRNAs without labeling, reducing cost and time and allowing testing in portable and affordable settings. EIS has been previously used to detect different miRNAs as well [36–40].

This paper presents an electrochemical biosensor specifically developed for the detection of miRNA-31. The principal component of the biosensor consists of a glassy carbon electrode, where graphene serves as the fundamental nanomaterial and single-stranded deoxyribonucleic acid (ssDNA) serves as the biorecognition element within the system. By employing this electrochemical biosensor platform, we propose an innovative electrochemical approach for the identification of miRNA-31 as a potential biomarker for oral cancer through EIS.

Experimental section

Materials

Graphene (X and Y Dimensions: > 2 μm and average thickness: 8–15 nm) from Cheap Tubes Incorporation, ethylenediamine tetraacetic acid (EDTA), potassium chloride (KCl), potassium dihydrogen phosphate (KH_2PO_4), and sodium phosphate monobasic anhydrous (NaH_2PO_4) from BDH[®], potassium ferrocyanide ($\text{K}_4[\text{Fe}(\text{CN})_6]$) and magnesium chloride hexahydrate ($\text{MgCl}_2 \cdot 6\text{H}_2\text{O}$) from MP Biomedicals; dimethylformamide (DMF) from Acros; potassium ferricyanide ($\text{K}_3[\text{Fe}(\text{CN})_6]$) from AMRESCO Inc.; 1-pyrenebutanoic acid succinimidyl ester (PBSE), and ethanolamine (EA) from Sigma-Aldrich; sodium phosphate dibasic anhydrous (Na_2HPO_4) and sodium chloride (NaCl) from EMD chemicals.

Milli-Q Millipore ultrapure deionized water (DI) with a resistivity value of 18 $\text{M}\Omega\text{-cm}$ was used for preparing all buffer solutions. The DNA and ribonucleic acid (RNA) oligonucleotides were purchased from Sigma Aldrich, and the stock solutions (100 μM) were prepared in DNase-RNase-free molecular grade water (Corning) and stored at $-80\text{ }^\circ\text{C}$. The working solution of DNA was prepared from the stock solutions, stored at -20

°C, and used during experiments to avoid any freeze/thaw cycle. DNase and RNase free filter pipette tips and microtubes were obtained from Olympus Plastics. All surfaces, including desiccators, were cleaned with 70% ethanol solution followed by RNaseZap solution to decontaminate any DNase or RNase residues. The following sequences of specific DNA and RNA oligonucleotides were used for the experiment:

ssDNA (probe DNA) 5'-NH₂-C₆- AGC TAT GCC AGC ATC TTG CCT - 3'.

Target miRNA-31 5'- AGG CAA GAU GCU GGC AUA GCU - 3'.

Non-complementary miRNA-25 5'- AGG CGG AGA CUU GGG CAA UUG - 3'.

Various buffers used throughout the experiments are as follows: A 10 mM Na₂HPO₄/NaH₂PO₄ phosphate buffer (PB) at a pH of 7.4 was used to wash the electrodes. An immobilization buffer (IB) containing 10 mM Na₂HPO₄/NaH₂PO₄ and 0.15 M NaCl was prepared to immobilize the ssDNA. Finally, a hybridization buffer (HB) was prepared by combining 10 mM PB, 1 M NaCl, and 20 mM MgCl₂ to hybridize miRNA on the electrode.

Electrochemical characterization

Electrochemical characterization was carried out using 1010E Interface (Gamry Instruments, Warminster, PA, USA). A three-electrode setup was implemented for the experiments. A 3 mm glassy carbon electrode (GCE), a platinum wire electrode, and 3 M Ag/AgCl were used as working, counter, and reference electrodes, and were purchased from CH Instruments Inc., Austin, TX, USA. All experiments were performed at room temperature using a 0.1 M KCl solution as an electrolyte containing 5 mM Fe(CN)₆^{3-/4-} solution in a 1:1 ratio. Cyclic voltammetry (CV) was performed between -0.2 V and 0.6 V and 20 mV/s as the scanning rate. An AC amplitude of 5 mV between 1 Hz and 100 kHz was used in EIS. The resulting measurements are presented as ΔR_{CT} and ΔR_{CT} (%) and copy number where NA is Avogadro's number ($6.023 \times 10^{23} \text{ mol}^{-1}$) and molecular weight of miRNA-31 is approximately 6890 g/mol:

$$\Delta R_{CT} = R_{CT}(\text{after hybridization}) - R_{CT}(\text{before hybridization})$$

$$\Delta R_{CT}(\%) = \frac{R_{CT}(\text{after hybridization}) - R_{CT}(\text{before hybridization})}{R_{CT}(\text{before hybridization})} \times 100\%$$

$$\text{Copy Number} = \frac{\text{Concentration} * NA}{\text{Molecular Weight (g/mol)}}$$

Fabrication of the electrode

A GCE was polished using 0.05 μm alumina powder for 5 min, and then the electrode was sonicated for 5 min in DI water to remove any residues of the polishing powder. The electrode was then thoroughly rinsed with DI water, dried in an oven at 70 °C for 45 min, and allowed to cool to room temperature. Simultaneously, a graphene solution was made by adding 1 mg of graphene to 10 mL DMF. The mixture was ultrasonicated using the ultra sonicator (Omni Sonic Ruptor 250, Omni International, Kennesaw, GA, USA) at 40 W for 30 min to form a homogenous dispersion. 2 μL of the graphene dispersion was dropped on the GCE surface and dried for an hour at room temperature to form a thin film as shown in Fig. 1. The advantage of drying at room temperature is that it prevents quick evaporation of the DMF and forms a more uniform coating.

Immobilizing ssDNA with a crosslinker

PBSE was used as the crosslinker to immobilize the ssDNA on a nanostructured electrode [41, 42]. 4 μL of 10 mM PBSE in DMF was incubated on the graphene-modified electrode for 15 min to allow the non-covalent binding between the graphene sheet and the aromatic pyrene rings of PBSE. The electrode was washed with DMF and PB sequentially to remove any unreacted PBSE molecules. A ssDNA electrode was developed by dropping 25 μL of DNA solution (2 μM in IB) and incubated for an hour at room temperature. The electrode was further treated with ethanolamine solution (10 mM in PB) for 30 min at room temperature to reduce non-specific sites and, lastly rinsed with PB to remove any unreacted DNA strands.

Hybridization with miRNAs

The electrode was rinsed once with the washing buffer, followed by a hybridization buffer to facilitate hybridization between the miRNA and ssDNA. 25 μL of miRNA-31 solution was deposited on the fabricated DNA immobilized electrode. The hybridizing time was set to an hour, and the electrode was rinsed with HB once and twice with PB to remove the non-hybridized miRNAs. The sensitivity was studied using different concentrations of miRNA-31 in buffer and two-fold diluted serum samples. A similar procedure was applied to non-complementary miRNA-25 to test the specificity of the biosensor in buffer and human serum samples. The specificity was tested using two-fold diluted serum samples and spiked with miRNA-31 and miRNA-25 [43–45]. All electrode modifications were analyzed using EIS analysis.

Results and discussion

Design and fabrication of the biosensor

The schematic diagram in Fig. 1 provides a detailed representation of the sequential steps in fabricating the electrochemical biosensor. The GCE served as the fundamental base platform and was modified with graphene through the physical adsorption method. The use of graphene as a nanomaterial serves to improve electronic properties while providing a larger surface area that accelerates electrode kinetics. This, in turn, helps in achieving a linear detection range and lower limit of detection (LOD) [46]. Additionally, the functionalization of graphene with biomolecules such as enzymes, antibodies, and DNA allows selective recognition of specific targets, which is essential for medical diagnostics [47]. PBSE was used as a covalent crosslinker for immobilizing ssDNA on the graphene-modified electrode, which has been previously reported by our research group [41, 42]. PBSE is highly effective because of π - π stacking interactions with graphene, which enables strong non-covalent interactions between the crosslinker and graphene-modified electrode, thereby preserving the high conductivity and surface properties of graphene [48, 49]. Other crosslinkers like 1-ethyl-3-(3-dimethylaminopropyl) carbodiimide (EDC) / N-hydroxysuccinimide (NHS) form covalent bonds, altering or reducing the surface properties, thereby affecting the overall performance of the

biosensor. In addition, PBSE forms stable covalent bonds with the amine groups of the DNA. The ester group reacts with the amine group on the ssDNA, providing a stronger and more stable attachment and enhancing the stability of the biosensor. Furthermore, the extensive use of PBSE in biosensors ensures that the DNA remains active and effectively binds to the target analyte [50].

Characterization of the electrochemical miRNA biosensor

The surface modification of the electrode with graphene and PBSE, as well as the immobilization of ssDNA and hybridization reactions, were evaluated by EIS and CV in a redox couple solution consisting of 5 mM $[\text{Fe}(\text{CN})_6]^{3/4}$ in 1:1 ratio in 0.1 M KCl. EIS was used to investigate the charge transfer properties of the developed electrode. Figure 2 shows the impedance spectra collected after each successive modification, presented as Nyquist plots. These Nyquist plots represent a semi-circular region at high frequencies, which indicates the electron transfer limiting processes at the electrode interface and a diffusion-controlled electrochemical process at lower frequencies. The EIS data were modeled using a Randles equivalent circuit. The interfacial electron transfer characteristics of the electrode were provided by R_{CT} values, estimated by measuring the diameter of the semi-circle in the Nyquist plot. Z-VIEW software (Scribner LLC, Southern Pines, NC) was used to calculate the value of the

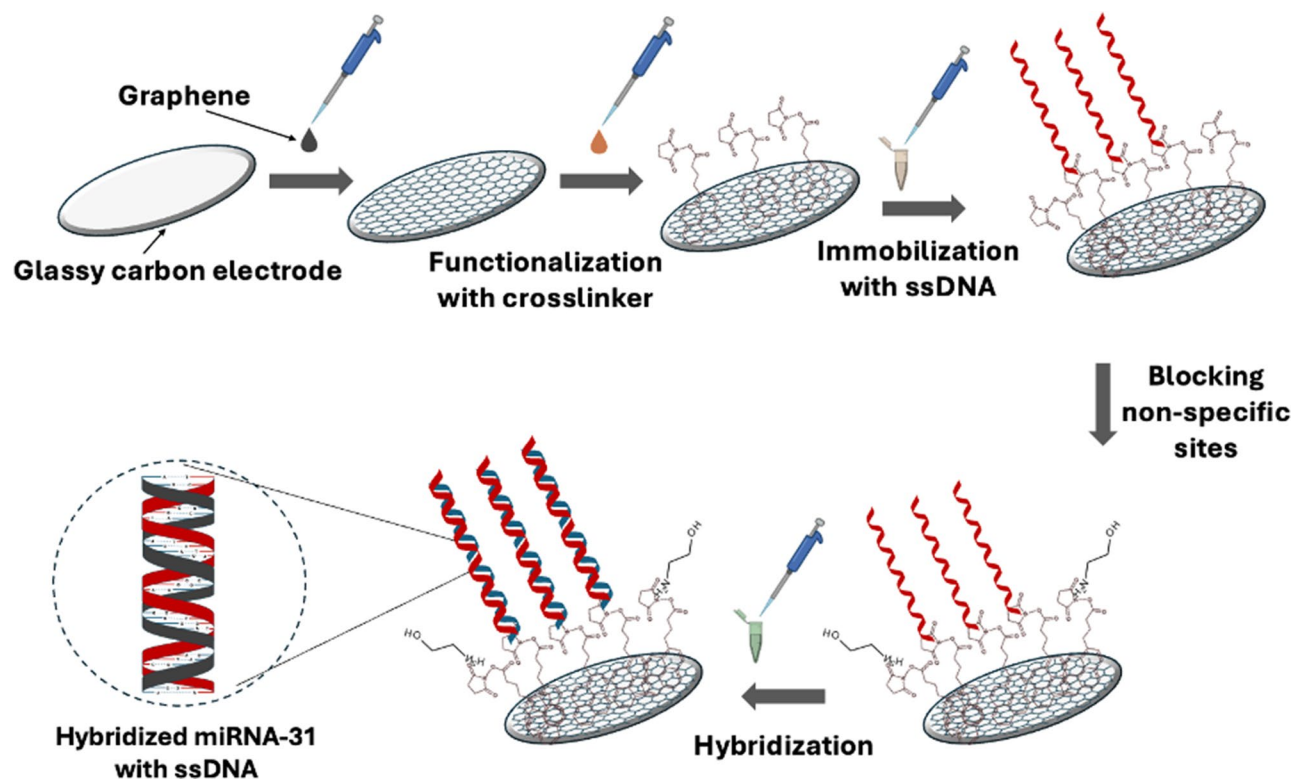


Fig. 1 The schematic representation of the fabrication principles for the developed biosensor

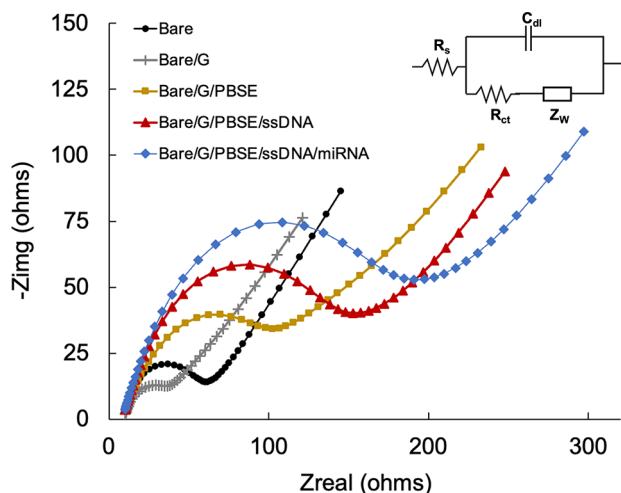


Fig. 2 Nyquist plots of different modified electrode surfaces performed in 0.1 M KCl with 5.0 mM $[\text{Fe}(\text{CN})_6]^{3-/4-}$. The inset shows the equivalent circuit used for fitting

equivalent circuit parameters. As shown in Fig. 2, the Nyquist plot shows a small semi-circle for the bare GCE; however, when the electrode was coated with graphene, the diameter of the semi-circle decreased. This phenomenon can be attributed to the conductive properties of graphene, which facilitate electron transfer and subsequently decrease R_{CT} .

As the electrode was further modified with PBSE, the R_{CT} increased due to the insulating properties of PBSE. The attachment of the ssDNA further increased the R_{CT} since the negatively charged DNA hinders the movement of the redox species [51]. Finally, the R_{CT} enlarges when the miRNA hybridizes with the ssDNA, reflecting the miRNA-31 binding to the DNA electrode surface. Furthermore, the stepwise CV results are depicted in Supplementary Fig. 1. The unmodified GCE displayed a reversible redox peak with a peak-to-peak separation of 120 mV, confirming an active and clean electrode surface. Incorporating graphene increased peak current density due to its high surface area and conductivity. Activating PBSE reduced current density because its hydrophobic nature hindered electron transfer. Immobilizing DNA further decreased current density and caused peak potential shifts, while successful miRNA binding through hybridization lowered the peak current.

Optimization of experimental conditions

Numerous critical parameters were rigorously evaluated to enhance the performance of the fabricated biosensor. Initially, to investigate the influence of graphene loading on the efficacy of the electrochemical biosensor, the working glassy carbon electrode was systematically modified with various concentrations of graphene solution. The electrochemical signal was recorded for each graphene loading to ascertain the required amount. The

results indicated a corresponding decline in the hybridization signal with increased graphene loading. This inverse relationship can be attributed to an excessive amount of graphene, which disrupts the sp^2 -hybridized carbon networks, thereby diminishing the overall conductivity of the electrode.

Furthermore, the presence of oxygen-containing functional groups at elevated concentrations of graphene may impede electron transfer processes, consequently reducing the sensitivity of the biosensor. Figure 3A illustrates the variation in signal responses corresponding to different graphene loadings. It is apparent that surpassing a certain threshold does not enhance and may indeed impair the performance of the sensor. Thus, an optimized graphene loading mass of $56 \mu\text{g}/\text{cm}^2$ was determined to achieve an optimal balance between sufficient conductive pathways and minimal interference from oxygen functional groups. This optimization ensures the biosensor maintains high sensitivity and reliability in microRNA detection.

Various concentrations of DNA loading were evaluated to enhance the immobilization of ssDNA on the fabricated electrode. This optimization process is critical, as inadequate DNA loading may lead to incomplete hybridization of DNA strands, while excessive loading can saturate the electrode surface, thereby hindering the specific binding of microRNA targets [52]. Moreover, overloading can result in false-positive signals, diminishing sensitivity and compromising detection accuracy. DNA concentrations ranging from $0.1 \mu\text{M}$ to $3 \mu\text{M}$ were analyzed in this investigation. The electrodes were hybridized with a target DNA concentration of $0.5 \mu\text{M}$ for an hour. Figure 3B illustrates the impedimetric measurements corresponding to different loadings of DNA. The optimal signal intensity was observed at a concentration of $2 \mu\text{M}$. As a result, a DNA concentration of $2 \mu\text{M}$ was designated as the optimal concentration for the biosensor platform. An optimal concentration of DNA is vital, as it facilitates the efficient capture of target molecules while minimizing steric hindrance and maintaining accessibility [53]. This balance enhances both the sensitivity and specificity of the biosensor. The chosen concentration of $2 \mu\text{M}$ has shown significant potential in achieving controlled DNA densities, thus optimizing the performance of the electrochemical DNA biosensor.

To comprehensively evaluate the effects of hybridization time on the performance of the biosensor, a series of timed tests were performed at intervals of 30 min, 45 min, 60 min, and 90 min. As illustrated in Fig. 3C, the impedimetric response, which quantifies the ability of the biosensor to detect miRNA, increased from 30 min to 60 min, indicating an improvement in hybridization efficiency. It is noteworthy that the signal began to decline following the 60-minute mark, with a substantial

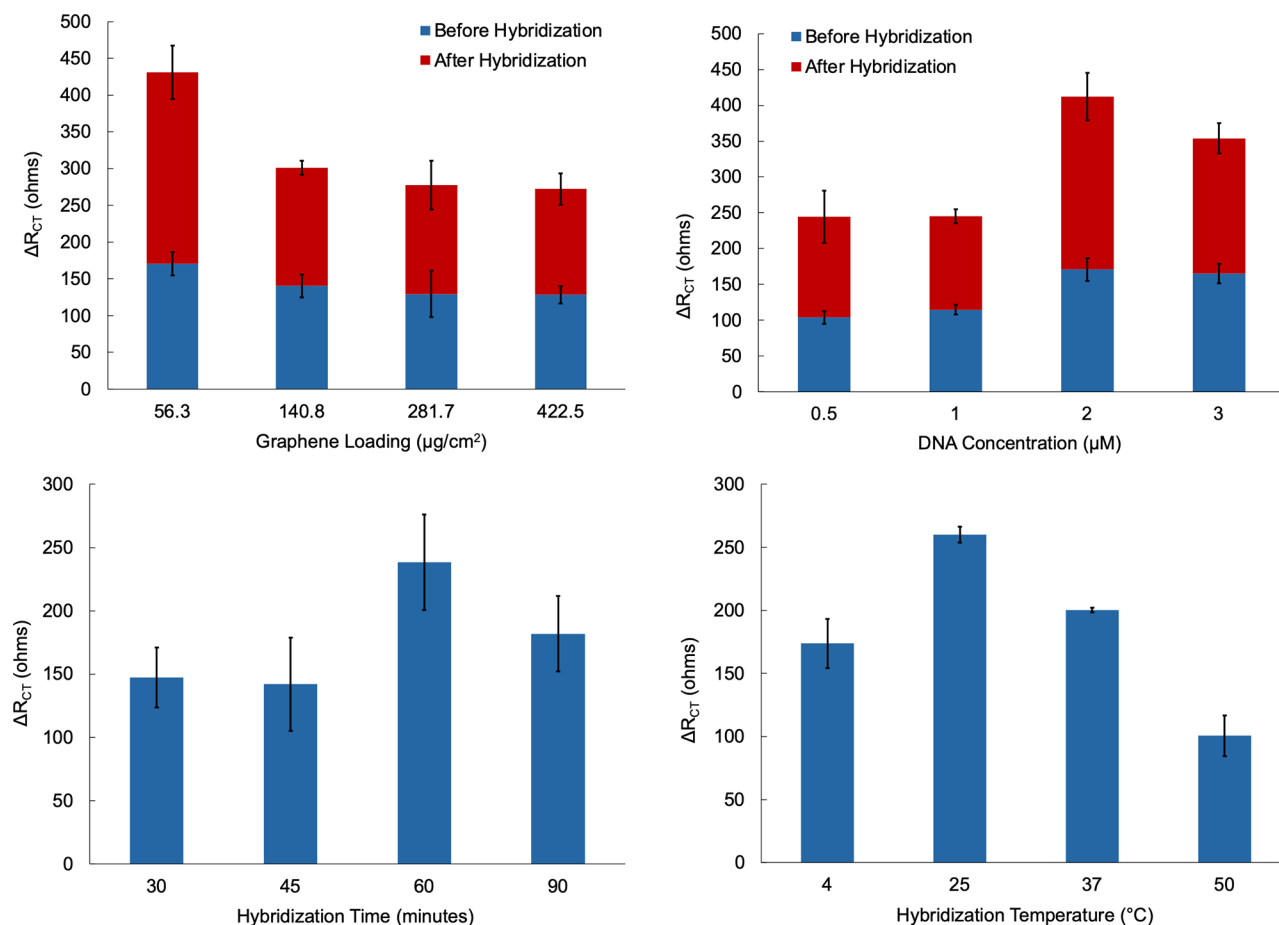


Fig. 3 Electrochemical impedance response for various optimization steps on the developed glassy carbon electrode. Graphene loading on the bare electrode and its effect in DRCT (A). DNA concentration and its effect in DRCT (B). RNA hybridization time and its impact in DRCT (C). RNA hybridization temperature and its effect in DRCT (D)

decrease recorded at 120 min. This decline can be attributed to the degradation of miRNA over time, which hampers its ability to bind effectively to the receptor on the biosensor surface. The degradation likely stems from enzymatic activity or thermal instability, which undermines the integrity of the miRNA, consequently reducing the hybridization signal [54]. Thus, based on the analyzed data, the optimal hybridization time is 60 min. This duration achieves a balance between maximal signal detection and the minimization of adverse effects due to miRNA degradation, thereby ensuring reliable and reproducible results for subsequent experiments.

The temperature plays a critical role in the hybridization process between miRNA and ssDNA molecules. To evaluate the influence of temperature on this hybridization reaction, experiments were conducted at four distinct temperatures: 4 $^{\circ}\text{C}$, 25 $^{\circ}\text{C}$, 37 $^{\circ}\text{C}$, and 50 $^{\circ}\text{C}$. Figure 3D illustrates the resulting hybridization signals, as determined by the variations in R_{CT} . As depicted in Fig. 3D, the R_{CT} values exhibited a progressive increase from 4 $^{\circ}\text{C}$ to 37 $^{\circ}\text{C}$, signifying an enhancement in

hybridization efficiency within this temperature range. This observation suggests that elevated temperatures facilitate the kinetic processes underlying hybridization, likely by increasing the molecular mobility and interaction rates of both miRNA and ssDNA molecules. Conversely, beyond 37 $^{\circ}\text{C}$, a reduction in the R_{CT} values was observed, with a significant decrease noted at 50 $^{\circ}\text{C}$. This decline can be attributed to the degradation of miRNA and the destabilization of the thermodynamic properties of the hybridized complex at elevated temperatures [55]. The instability associated with higher temperatures prompts the dissociation of the ssDNA-miRNA complex, diminishing the hybridization signal. It is noteworthy that the signal variation between 25 $^{\circ}\text{C}$ and 37 $^{\circ}\text{C}$ was minimal, indicating a stable hybridization environment within this temperature range. However, a slight decrease was observed, potentially due to partial destabilization at the upper end of this range. Based on these findings, 25 $^{\circ}\text{C}$ is the optimal temperature for hybridization experiments. This temperature strikes an equilibrium between efficient hybridization kinetics and the stability of the

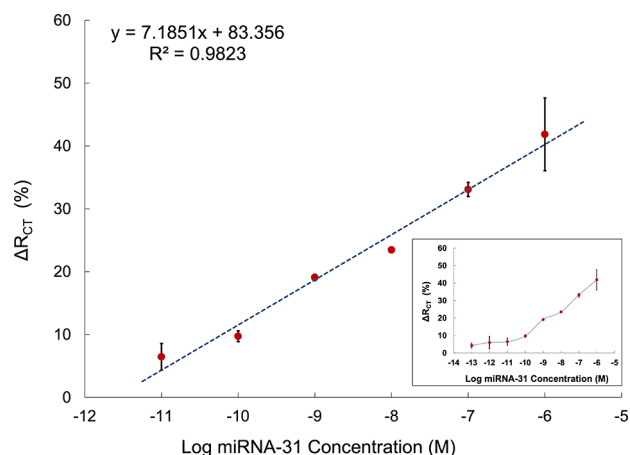


Fig. 4 The sensitivity calibration curve is based on the relationship between ΔR_{CT} (%) and the logarithmic concentration of miRNA-31 in buffer. The inset shows the full calibration curve of the concentration range

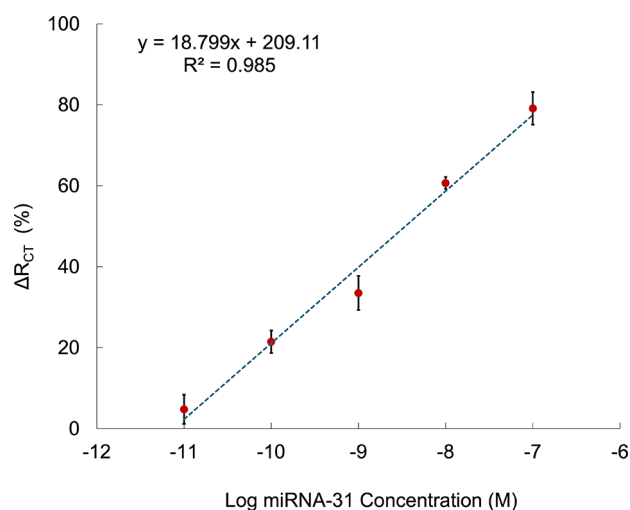


Fig. 5 The sensitivity calibration curve is based on the relationship between ΔR_{CT} (%) and the logarithmic concentration of miRNA-31 in diluted serum

miRNA-ssDNA complex, thereby ensuring reliable and reproducible results without significant degradation or dissociation [56]. Moreover, the overall detection time is under 5 min, making it faster than isothermal NAATs and other existing methods [26, 27].

Sensitivity of the biosensor

In conducting sensitivity studies, the analytical performance of the biosensors was assessed using varying concentrations of miRNA-31 under optimized conditions. Figures 4 and 5 presents the calibration curve, constructed on the average of ΔR_{CT} (%) plotted against the logarithmic values of miRNA-31 concentrations in buffer and diluted serum respectively. The performance of the developed biosensor was compared with previously published miRNA detection studies, which are summarized

in Table 1. In addition, this data was compared with other target and sensing methods used for oral cancer detection as in shown in Table 2. Furthermore, the linear range of detection is comparable to other biosensors reported in the literature. The calibration curve indicated a linear relationship within the concentration range of 10^{-11} M to 10^{-6} M in buffer and 10^{-11} M to 10^{-7} M in diluted serum. The detection limit was determined to be 10^{-11} M in buffer (70 pg/mL or 6.022×10^6 copies/ μ L), 10^{-10} M in diluted serum (700 pg/mL or 6.022×10^7 copies/ μ L) and 10^{-8} M in undiluted serum (0.07 pg/mL or 6.022×10^9 copies/ μ L) for the complementary target miRNA-31 using the Six Sigma method [57, 58]. Additionally, the resulting linear equation is represented as ΔR_{CT} (%) = $7.185 \log C_{miRNA-31} + 83.356$ in buffer, accompanied by a correlation coefficient of 0.9823 and ΔR_{CT} (%) = $18.799 \log C_{miRNA-31} + 209.11$ in serum, accompanied by a correlation coefficient of 0.985. The limit of detection was found to be 2.6×10^{-12} M (18.2 pg/mL or 1.56×10^9 copies/ μ L) in buffer and 0.7×10^{-12} M (4.9 pg/mL or 4×10^8 copies/ μ L) in diluted serum using the regression equation: $3.3 \times SD / s$ (where SD is the standard deviation of the intercept and s is the slope of the calibration curve). To date, the modified glassy carbon electrode-based electrochemical biosensor has not been documented for the sensitive detection of oral cancer utilizing miRNA-31 as a potential biomarker. Thus, the developed biosensor demonstrates significant advantages in terms of sensitivity. The LOD indicates that the current biosensor offers a broad linear range while providing several practical benefits in design and usability. This further enhances its potential for detecting miRNA-31 as a potential biomarker for oral cancer, facilitating early diagnosis and aiding in additional confirmation in clinical decision-making.

Specificity of the biosensor

The electrochemical biosensor exhibits remarkable sensitivity for the detection of miRNA-31. However, a critical analysis is required to enhance the specificity of the biosensor, allowing for the differentiation of miRNA-31 from other related biomolecules. To verify the specificity of the biosensor, miRNA-25, a non-complementary nucleotide, was employed to conduct a hybridization reaction and was subsequently compared to the complementary miRNA-31 at a concentration of 10^{-7} M. Despite their mutual association with cancer, the developed biosensor strategically leverages the distinctions between miRNA-31 and miRNA-25. As illustrated in Fig. 6, a significant increase was recorded in the R_{CT} value between miRNA-25 and miRNA-31 across two distinct samples. The complementary miRNA demonstrated an increase in impedance of 59% in buffer and 82% in serum compared to the non-complementary strand, thereby confirming

Table 1 A comparative analysis of the fabricated MiRNA biosensor in relation to other documented electrochemical biosensors for MiRNA detection

| Electrode | Recognition element | Target | Signaling element | Electrochemical technique | LOD | References |
|---------------------|--|-----------|---|---------------------------|----------------------------------|------------------|
| Pencil graphite | MWCNTs | miRNA-125 | [Fe(CN) ₆] ^{3-/4-} | EIS | 10 pM | [61] |
| Glassy carbon | MoS ₂ /Thi/AuNPs | miRNA-21 | Thionine | SWV | 0.26 pM | [62] |
| Glassy carbon | Graphene/PBSE | miRNA-21 | [Fe(CN) ₆] ^{3-/4-} | EIS | 3 fM | [41] |
| FTO | SWCNTs den-Au | miRNA-21 | [Fe(CN) ₆] ^{3-/4-} | DPV | 0.01 fM | [63] |
| HRCA-strip platform | (StrepMBs) with biotin-modified DNA probes | miRNA-31 | [Fe(CN) ₆] ^{3-/4-} | - | 3.21 fM | [64] |
| Gold | MCH | miRNA-21 | [Fe(CN) ₆] ^{3-/4-} | DPV/EIS | 0.6 pM | [65] |
| Paper | AuNPs/rGO | miRNA-21 | [Fe(CN) ₆] ^{3-/4-} | DPV | 12 nM | [66] |
| Paper | AuNPs/rGO | miRNA-155 | [Fe(CN) ₆] ^{3-/4-} | DPV | 25.7 nM | [66] |
| Glassy carbon | Graphene | miRNA-31 | [Fe(CN) ₆] ^{3-/4-} | EIS | 10 pM (buffer) 100 pM (serum) | This work |

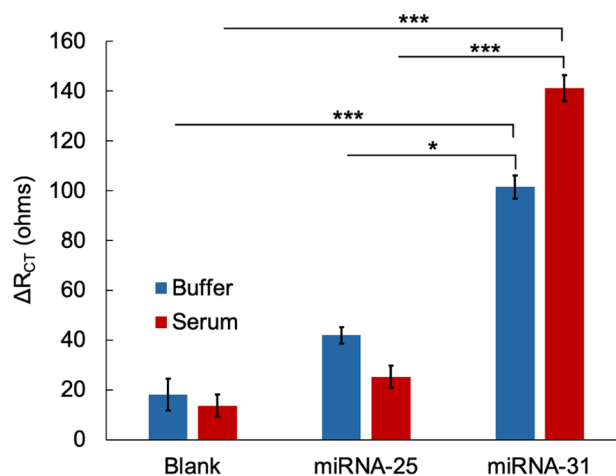
MWCNTs, multi walled carbon nanotubes; EIS, electrochemical impedance spectroscopy; MoS₂, Molybdenum disulfide; Thi, thionine; AuNPs, gold nanoparticles; SWV, square-wave voltammetry; PBSE, 1-pyrenebutyric acid-N-hydroxysuccinimide ester; FTO, fluorine-doped tin oxide; SWCNTs, single walled carbon nanotubes, den-Au, dendritic gold; DPV, differential pulse voltammetry; HRCA, hyper-branched rolling circle amplification; StrepMBs, Group B *Streptococcus* magnetic beads; MCH, Melanin-concentrating hormone; rGO, reduced graphene oxide

Table 2 A comparison table of various targets with different sensing methods for the detection of oral cancer biomarkers

| Biomarker | Method | Analyte | Detection limit | References |
|------------|-------------------|--------------------------|---------------------------|------------------|
| IL-8 | CV/EIS | Human Serum and Saliva | 3.3 fg/mL | [67] |
| IL-6 | Amperometry | Human serum | 0.5 pg/mL | [68] |
| MMP-7 | Amperometry | Human serum | 1 ng/mL | [69] |
| ORAOV1 | CV/DPV | Artificial saliva | 3 fg/mL | [70] |
| miRNA-200a | Chronoamperometry | Artificial saliva | 2.2 × 10 ⁻¹⁹ M | [71] |
| HIF-1α | Amperometry | Human saliva | 76 pg/mL | [72] |
| miRNA-31 | EIS | Buffer Human serum | 70 pg/mL 700 pg/mL | This work |

Abbreviations IL-8 - Interleukin-8, IL-6 - Interleukin-6, MMP-7 - Matrix Metalloproteinase-7, ORAOV1 - Oral cancer overexpressed 1, HIF-1α - Hypoxia-inducible factor 1-alpha, CV - Cyclic Voltammetry, EIS - Electrochemical Impedance Spectroscopy, DPV - Differential Pulse Voltammetry

the sequence-specific binding between ssDNA and miRNA-31. Furthermore, established clinical protocols and assays for serum make it a consistent and standardized option for early detection and monitoring of oral cancers [59, 60]. The pronounced dissimilarities between miRNA-31 and miRNA-25 facilitate precise detection in both serum and buffer analytes, thereby enhancing the accuracy of the developed biosensor in identifying OSCC biomarkers. These findings substantiate the predicted level of specificity of the biosensor while also indicating potential areas for improvement, such as reducing the non-specific adsorption on the ssDNA.

**Fig. 6** Specificity studies of the target miRNA-31 and non-complementary miRNA-25 in buffer and diluted serum. The asterisks indicate statistical significance (* $p < 0.05$, and *** $p < 0.001$ using a two-tailed test)

Time stability of the biosensor

The electrochemical stability of the biosensor was systematically evaluated subsequent to the preparation of the electrode. PBS was utilized to store the PBSE-modified immobilized electrodes at 4 °C for varying durations, specifically 1 h, 24 h, 3 days, 7 days, and 10 days. Following each storage interval, impedance measurements were taken at a concentration of 10⁻⁷ M in triplicate alongside impedance measurements. The R_{CT} value was quantified, and the ΔR_{CT} was calculated to the response measured after an hour. As illustrated in Fig. 7, the biosensor demonstrated stability after 3 days, exhibiting only a 70% reduction in signal relative to the response recorded an hour post-preparation. A low error value suggests that the performance of the sensor is repeatable after a week. After 10 days, the reduction in the signal was 60% with

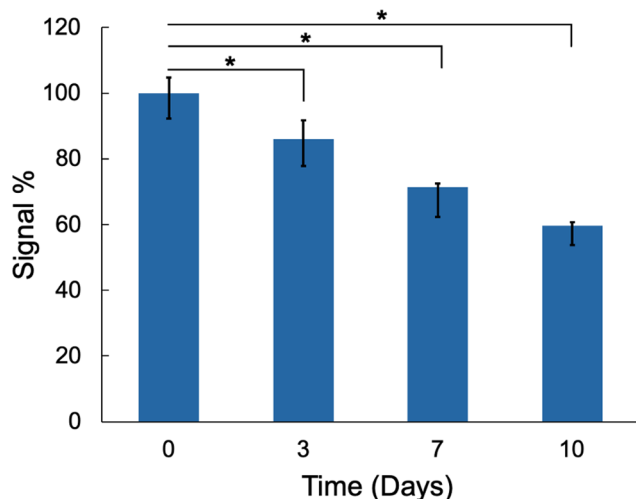


Fig. 7 Time stability studies of the developed biosensor with 10^{-7} M miRNA-31. The asterisk indicates statistical significance ($* p < 0.05$ using a two-tailed test)

$\pm 7\%$ error margin. The signals exhibit a marked decline beyond 10 days, indicating that they may become less stable and inaccurate.

Conclusions

The application of miRNA-31 as a non-invasive potential biomarker for the early detection of oral cancer has been developed and evaluated using an ultra-sensitive biosensor platform. This biosensor has enhanced sensitivity and specificity through meticulous optimization of graphene loading on the electrode surface, DNA concentration, hybridization duration, and hybridization temperature. Comprehensive optimization procedures have significantly enhanced the LOD while minimizing non-specific interactions, thereby ensuring reliable and accurate detection outcomes. It has been demonstrated that the biosensor can detect the target analyte with a limit of detection of 10^{-11} M (70 pg/mL or 6.022×10^6 copies/ μ L) in buffer and 10^{-10} M (700 pg/mL or 6.022×10^7 copies/ μ L) in diluted serum for the complementary target miRNA-31 using the Six Sigma method. Furthermore, the biosensor exhibits a high degree of specificity toward complementary miRNA-31 and demonstrates remarkable stability and applicability in serum samples. In addition, the biosensor offers key advantages over existing technologies, such as shorter detection time and use of inexpensive reagents. The performance of the biosensor may be influenced by various factors, including fluctuations in incubation temperature throughout the hybridization process and the degradation of bioreceptors over time. Therefore, a critical analysis indicates a necessity for further investigation into the long-term stability of

the biosensor to address potential challenges associated with real-world applications. Future research could involve assessing the biosensor's performance with real samples, further enhancing point-of-care diagnostics and personalized treatment strategies for individuals with oral cancer. Its early detection capability may serve as an initial screening tool, offering a reliable and sensitive confirmation. For a comprehensive diagnosis, established methods like qPCR could be used as additional validation tools, complementing the biosensor's detection capability and improving overall diagnostic accuracy.

Abbreviations

| | |
|----------|--|
| C_{DL} | Double-layer Capacitance |
| CV | Cyclic Voltammetry |
| DdPCR | Droplet Digital Polymerase Chain Reaction |
| DI | Deionized Water |
| DNA | Deoxyribonucleic Acid |
| EDC | 1-ethyl-3-(3-dimethylaminopropyl) carbodiimide |
| EIS | Electrochemical Impedance Spectroscopy |
| GCE | Glassy Carbon Electrode |
| HB | Hybridization Buffer |
| HPV | Human Papillomavirus |
| IB | Immobilization Buffer |
| LOD | Limit of Detection |
| miRNA | microRNA |
| NAATs | Nucleic Acid Amplification Techniques |
| NHS | N-hydroxysuccinimide |
| OSCC | Oral Squamous Cell Carcinoma |
| PB | Phosphate Buffer |
| PBSE | 1-Pyrenebutyric acid N-hydroxysuccinimide ester |
| R_{CT} | Charge Transfer Resistance |
| RNA | Ribonucleic Acid |
| R_s | Solution Resistance |
| RT-qPCR | Reverse Transcription Quantitative Polymerase Chain Reaction |
| ssDNA | Single Stranded Deoxyribonucleic Acid |
| Z_w | Warburg Resistance |

Supplementary Information

The online version contains supplementary material available at <https://doi.org/10.1186/s13036-025-00492-1>.

Supplementary Material 1

Acknowledgements

Not applicable.

Author contributions

Conceptualization, S.N.N. and R.P.R.; methodology, S.N.N. and R.P.R.; software, S.N.N.; validation, S.N.N., B.S. and R.P.R.; formal analysis, S.N.N., B.S. and R.P.R.; investigation, S.N.N., B.S. and R.P.R.; resources, R.P.R.; data curation, S.N.N.; writing—original draft, S.N.N. and B.S.; writing—review and editing, S.N.N., B.S. and R.P.R.; visualization, S.N.N., B.S. and R.P.R.; supervision, B.S. and R.P.R.; project administration, R.P.R. All authors reviewed the manuscript.

Funding

This research received no funding.

Data availability

The authors confirm that the data supporting the findings of this study are available within the article and its Supplementary Materials. The data that support the findings of this study are available from the corresponding author, Ramaraja Ramasamy, upon reasonable request.

Declarations

Ethics approval and consent to participate

Not applicable.

Consent for publication

Not applicable.

Competing interests

The authors declare no competing interests.

Author details

¹Nano Electrochemistry Laboratory, School of Chemical, Materials, and Biomedical Engineering, University of Georgia, Athens 30602, USA

Received: 13 December 2024 / Accepted: 28 February 2025

Published online: 25 March 2025

References

1. Sun RY, et al. Global, regional, and National burden of oral cancer and its attributable risk factors from 1990 to 2019. *Cancer Med*. 2023;12(12):13811–20.
2. Hernandez-Morales A et al. Lip and oral cavity Cancer incidence and mortality rates associated with smoking and chewing tobacco use and the human development index in 172 countries worldwide: an ecological study 2019–2020. *Healthcare (Basel)*. 2023. 11(8).
3. Shahid A, et al. Hidden wonders in a Spit: novel technologies for salivary diagnostics. *J Indian Acad Oral Med Radiol*. 2020;32(1):41–5.
4. Tan YH et al. Oral squamous cell carcinomas: state of the field and emerging directions. *Int J Oral Sci*. 2023. 15(1).
5. Sahibzada HA et al. Salivary IL-8, IL-6 and TNF-alpha as potential diagnostic biomarkers for oral Cancer. *Diagnostics (Basel)*. 2017. 7(2).
6. Ferrari E et al. Salivary cytokines as biomarkers for oral squamous cell carcinoma: A systematic review. *Int J Mol Sci*. 2021. 22(13).
7. Mumtaz M, et al. Secreted protein markers in oral squamous cell carcinoma (OSCC). *Clin Proteom*. 2022;19(1):4.
8. Chakraborty A et al. MiRNAs: potential as biomarkers and therapeutic targets for Cancer. *Genes*. 2023. 14(7).
9. Lan HY et al. MicroRNAs as Potential Biomarkers in Cancer: Opportunities and Challenges. *Biomed Research International*, 2015. 2015.
10. Wang J, et al. Diagnostic and therapeutic role of MicroRNAs in oral cancer (Review). *Oncol Rep*. 2021;45(1):58–64.
11. Osan C et al. The connection between MicroRNAs and oral Cancer pathogenesis: emerging biomarkers in oral Cancer management. *Genes (Basel)*. 2021. 12(12).
12. Yu EH, et al. MicroRNA-21 promotes perineural invasion and impacts survival in patients with oral carcinoma. *J Chin Med Assoc*. 2017;80(6):383–8.
13. He L, et al. Salivary Exosomal miR-24-3p serves as a potential detective biomarker for oral squamous cell carcinoma screening. *Biomedicine & Pharmacotherapy*; 2020, p. 121.
14. Lu ZY, et al. miR-31-5p is a potential Circulating biomarker and therapeutic target for oral Cancer. *Mol Therapy-Nucleic Acids*. 2019;16:471–80.
15. Khijmatgar S, et al. Salivary biomarkers for early detection of oral squamous cell carcinoma (OSCC) and head/neck squamous cell carcinoma (HNSCC): A systematic review and network meta-analysis. *Jpn Dent Sci Rev*. 2024;60:32–9.
16. Riccardi G et al. Salivary biomarkers in oral squamous cell carcinoma: A proteomic overview. *Proteomes*. 2022. 10(4).
17. Wang LL, et al. MiR-31 is a potential biomarker for diagnosis of head and neck squamous cell carcinoma. *Int J Clin Exp Pathol*. 2018;11(9):4339–45.
18. Kumari P, et al. Expression of miR-31 in saliva-liquid biopsy in patients with oral squamous cell carcinoma. *J Taibah Univ Med Sci*. 2021;16(5):733–9.
19. Fernandez-Olavarria A, et al. The role of serum biomarkers in the diagnosis and prognosis of oral cancer: A systematic review. *J Clin Exp Dent*. 2016;8(2):e184–93.
20. Towle R, et al. Identification of a serum-based MicroRNA signature that detects recurrent oral squamous cell carcinoma before it is clinically evident. *Br J Cancer*. 2023;129(11):1810–7.
21. Stepicheva NA, Song JL. Function and regulation of microRNA-31 in development and disease. *Mol Reprod Dev*. 2016;83(8):654–74.
22. Dziadkowiak E et al. miR-31-5p as a Potential Circulating Biomarker and Tracer of Clinical Improvement for Chronic Inflammatory Demyelinating Polyneuropathy. *Oxid Med Cell Longev*. 2023. 2023: p. 2305163.
23. Shahbazi-Derakhshi P et al. An ultrasensitive miRNA-Based genosensor for detection of MicroRNA 21 in gastric Cancer cells based on functional signal amplifier and synthesized Perovskite-Graphene oxide and AuNPs. *Biosens (Basel)*. 2023. 13(2).
24. El Aamri M et al. Electrochemical biosensors for detection of MicroRNA as a Cancer biomarker: pros and cons. *Biosensors-Basel*. 2020. 10(11).
25. Ye J, et al. Research advances in the detection of MiRNA. *J Pharm Anal*. 2019;9(4):217–26.
26. Narasimhan V, et al. Nucleic acid Amplification-Based technologies (NAAT)—Toward accessible, autonomous, and mobile diagnostics. *Adv Mater Technol*. 2023;8(20):2300230.
27. Oliveira BB, Veigas B, Baptista PV. Isothermal amplification of nucleic acids: the race for the next gold standard. *Front Sens*. 2021. 2.
28. Aziz A, et al. Trends in biosensing platforms for SARS-CoV-2 detection: A critical appraisal against standard detection tools. *Curr Opin Colloid Interface Sci*. 2021;52:101418.
29. Craw P, Balachandran W. Isothermal nucleic acid amplification technologies for point-of-care diagnostics: a critical review. *Lab Chip*. 2012;12(14):2469–86.
30. Metcalf GAD. MicroRNAs: Circulating biomarkers for the early detection of imperceptible cancers via biosensor and machine-learning advances. *Oncogene*. 2024;43(28):2135–42.
31. Catuogno S, et al. Recent advance in biosensors for MicroRNAs detection in Cancer. *Cancers (Basel)*. 2011;3(2):1877–98.
32. Sethuraman S, et al. Nanomaterial biosensors in salivary diagnosis of oral cancer: A scoping review. *Cureus*. 2024;16(5):e59779.
33. Martino S et al. MicroRNA detection via nanostructured biochips for early Cancer diagnostics. *Int J Mol Sci*. 2023. 24(9).
34. Kaur D, Esseili MA, Ramasamy RP. A Cell-Based electrochemical biosensor for the detection of infectious hepatitis A virus. *Biosensors*. 2024;14(12):576.
35. Magar HS, Hassan RYA, Mulchandani A. Electrochemical impedance spectroscopy (EIS): principles, construction, and biosensing applications. *Sens (Basel)*. 2021. 21(19).
36. Jolly P, et al. Highly sensitive dual mode electrochemical platform for MicroRNA detection. *Sci Rep*. 2016;6:36719.
37. Meng T, et al. Construction of an ultrasensitive electrochemical sensing platform for microRNA-21 based on interface impedance spectroscopy. *J Colloid Interface Sci*. 2020;578:164–70.
38. Ustuner S, Lindsay MA, Estrela P. Pre-concentration of MicroRNAs by LNA-modified magnetic beads for enhancement of electrochemical detection. *Sci Rep*. 2021;11(1):19650.
39. Han S, et al. Facile and Label-Free electrochemical biosensors for MicroRNA detection based on DNA Origami nanostructures. *ACS Omega*. 2019;4(6):11025–31.
40. Roychoudhury A, et al. Circulating MicroRNA detection using electrochemical biosensor for rapid diagnosis of liver disease in dogs. *Sens Diagnostics*. 2024;3(7):1190–200.
41. Asadi H, Ramasamy RP. Graphene-based electrochemical biosensor for impedimetric detection of MiRNAs as potential Cancer biomarkers. *J Electrochem Soc*. 2020. 167(16).
42. Hansen L et al. An electrochemical nucleic acid biosensor for Triple-Negative breast Cancer biomarker detection. *Sens (Basel)*. 2024. 24(17).
43. Hu TX, et al. Enzyme catalytic amplification of miRNA-155 detection with graphene quantum dot-based electrochemical biosensor. *Biosens Bioelectron*. 2016;77:451–6.
44. Zouari M, et al. Amperometric biosensing of miRNA-21 in serum and Cancer cells at nanostructured platforms using Anti-DNA-RNA hybrid antibodies. *ACS Omega*. 2018;3(8):8923–31.
45. Cai SL et al. Single-molecule amplification-free multiplexed detection of Circulating MicroRNA cancer biomarkers from serum. *Nat Commun*. 2021. 12(1).
46. Bai Y, Xu T, Zhang X. Graphene-Based biosensors for detection of biomarkers. *Micromachines (Basel)*. 2020. 11(1).
47. Shahriari S, et al. Graphene and graphene oxide as a support for biomolecules in the development of biosensors. *Nanotechnol Sci Appl*. 2021;14:197–220.
48. Hunter CA, Sanders JKM. The nature of Pi-Pi interactions. *J Am Chem Soc*. 1990;112(14):5525–34.
49. Oishi Y, et al. Theoretical analysis on the stability of 1-Pyrenebutanoic acid succinimidyl ester adsorbed on graphene. *ACS Omega*. 2022;7(35):31120–5.

50. Suvarnaphaet P, Pechprasarn S. Graphene-Based materials for biosensors: A review. *Sens (Basel)*. 2017. 17(10).
51. Genereux JC, Boal AK, Barton JK. DNA-mediated charge transport in redox sensing and signaling. *J Am Chem Soc*. 2010;132(3):891–905.
52. Keighley SD, et al. Optimization of label-free DNA detection with electrochemical impedance spectroscopy using PNA probes. *Biosens Bioelectron*. 2008;24(4):912–7.
53. White RJ, et al. Optimization of electrochemical aptamer-based sensors via optimization of probe packing density and surface chemistry. *Langmuir*. 2008;24(18):10513–8.
54. Zhou L, et al. A label-free electrochemical biosensor for MicroRNAs detection based on DNA nanomaterial by coupling with Y-shaped DNA structure and non-linear hybridization chain reaction. *Biosens Bioelectron*. 2019;126:657–63.
55. Wu P, Nakano S, Sugimoto N. Temperature dependence of thermodynamic properties for DNA/DNA and RNA/DNA duplex formation. *Eur J Biochem*. 2002;269(12):2821–30.
56. Abdul Rashid JJ, et al. Strategies in the optimization of DNA hybridization conditions and its role in electrochemical detection of dengue virus (DENV) using response surface methodology (RSM). *RSC Adv*. 2023;13(27):18748–59.
57. Looock HP, Wentzell PD. Detection limits of chemical sensors: applications and misapplications. *Sens Actuators B-Chemical*. 2012;173:157–63.
58. Pyzdek T, Keller PA. *The six sigma handbook*. Fourth edition. ed. 2014, New York: McGraw-Hill Education. xiv, 690 pages.
59. Wu YH, et al. Serum levels and positive rates of tumor biomarkers in oral precancer patients. *J Formos Med Assoc*. 2021;120(6):1324–31.
60. Liu W, et al. Causal association of serum biomarkers with oral cavity and oropharyngeal cancer: a Mendelian randomization study. *BMC Oral Health*. 2023;23(1):987.
61. Yammouri G, et al. Development of an electrochemical label-free biosensor for microRNA-125a detection using pencil graphite electrode modified with different carbon nanomaterials. *J Electroanal Chem*. 2017;806:75–81.
62. Zhu D, et al. Label-Free electrochemical sensing platform for MicroRNA-21 detection using Thionine and gold nanoparticles Co-Functionalized MoS(2) nanosheet. *ACS Appl Mater Interfaces*. 2017;9(41):35597–603.
63. Sabahi A, et al. Electrochemical nano-genosensor for highly sensitive detection of miR-21 biomarker based on SWCNT-grafted dendritic Au nanostructure for early detection of prostate cancer. *Talanta*. 2020;209:120595.
64. Li W, et al. A lateral flow strip biosensor platform based on cascade nucleic acid amplification technology for ultrasensitive detection of OSCC-associated salivary MicroRNA. *Anal Chim Acta*. 2022;1221:340112.
65. Zhang Y, et al. A simple electrochemical biosensor for highly sensitive and specific detection of MicroRNA based on mismatched catalytic hairpin assembly. *Biosens Bioelectron*. 2015;68:343–9.
66. Torul H et al. Paper-Based Electrochemical Biosensors for Voltammetric Detection of miRNA Biomarkers Using Reduced Graphene Oxide or MoS(2) Nanosheets Decorated with Gold Nanoparticle Electrodes. *Biosensors (Basel)*. 2021. 11(7).
67. Aydin M, Aydin EB, Sezginurk MK. A highly selective electrochemical immunosensor based on conductive carbon black and star PGMA polymer composite material for IL-8 biomarker detection in Human Serum and Saliva. *Biosens Bioelectron*. 2018;117:720–8.
68. Malhotra R, et al. Ultrasensitive electrochemical immunosensor for oral Cancer biomarker IL-6 using carbon nanotube forest electrodes and multilabel amplification. *Anal Chem*. 2010;82(8):3118–23.
69. Wei Z et al. Amperometric biosensor of matrix Metalloproteinase-7 enhanced by Pd-Functionalized carbon nanocomposites. *Nanoscale Res Lett*. 2018. 13.
70. Hu YR, et al. An electrochemical biosensor for detection of DNA species related to oral Cancer based on a particular Host-Guest Recognition-Assisted strategy for signal Tag in situ. *J Electrochem Soc*. 2018;165(7):B289–95.
71. Wang ZW, et al. A novel electrically magnetic-controllable electrochemical biosensor for the ultra sensitive and specific detection of attomolar level oral cancer-related MicroRNA. *Biosens Bioelectron*. 2013;45:108–13.
72. Muñoz-San Martín C et al. Magnetic beads-based electrochemical Immunosensing of HIF-1 α , a biomarker of tumoral hypoxia. *Sens Actuators B-Chemical*, 2020. 307.

Publisher's note

Springer Nature remains neutral with regard to jurisdictional claims in published maps and institutional affiliations.